Diffusion Measurement of Fluorescence-Labeled Amphiphilic Molecules with a Standard Fluorescence Microscope

Christian Dietrich,*# Rudolf Merkel,* and Robert Tampé*§
*Physics Department, Biophysics Group, Technische Universität München, D-85478 Garching, Germany; #Centre de Recherche Paul Pascal, CNRS, F-33600 Pessac, France; and §Max-Planck-Institut für Biochemie, D-82152 Martinsried, Germany

ABSTRACT The lateral diffusion of fluorescence-labeled amphiphilic tracer molecules dissolved within a two-dimensional matrix of lipids was measured by continuous illumination of an elongated rectangular region. The resulting spatial concentration profile of unbleached tracer molecules was observed with a standard epifluorescence microscope and analyzed with digital image-processing techniques. These concentration profiles are governed by the mobility of the tracers, their rate of photolysis, and the geometry of the illuminated area. For the case of a long and narrow illuminated stripe, a mathematical analysis of the process is given. After prolonged exposure, the concentration profile can be approximated by a simple analytical function. This fact was used to measure the quotient of the rate of photolysis and the diffusion constant of the fluorescent probe. With an additional measurement of the rate of photolysis, the mobility of the tracer was determined. As prototype experiments we studied the temperature dependence of the lateral diffusion of *N*-(7-nitrobenz-2-oxa-1,3-diazol-4-yl)-dipalmitoylphosphatidyl ethanolamine in glass-supported bilayers of L-α-dimyristoylphosphatidylcholine. Because of its simple experimental setup, this technique represents a very useful method of determining the lateral diffusion of fluorescence-labeled membrane molecules.

INTRODUCTION

The mobility of molecules within a two-dimensional fluid is of great interest in many fields of research. Diffusion of lipids and proteins is relevant for physiological processes in native membranes (Jacobson et al., 1995; Cherry, 1979). In model systems, such as artificial lipid bilayers, monolayers at the air-water interface, solid-supported planar bilayers, or recently introduced polymer supported lipid layers, the diffusion of lipids or dissolved molecules is a sensitive indicator of phase state and connectivity (Peters and Beck, 1983; Tamm and McConnell, 1985; Vaz et al., 1985; Kühner et al., 1994). For these reasons a large number of techniques have been developed to investigate lateral diffusion of molecules in lipid layers.

A classical approach is to dope the lipid matrix with fluorescent probes and measure the diffusivity of these probes. The common assumption is that the mobility of the tracer molecules is representative of the mobility of the surrounding lipid matrix. The basic idea of fluorescence recovery after photobleaching (FRAP) and derived techniques is to irreversibly bleach the fluorescent probes in a defined area with a high-intensity light flash and to monitor the subsequent fluorescence recovery. These techniques, such as FRAP (Axelrod et al., 1976), total internal reflection-FRAP (Thompson et al., 1981), pattern photobleaching (Smith and McConnell, 1978; Miehlich and Gaub, 1993), and scanning microphotolysis (SCAMP) (Wedekind et al., 1994) allow high-accuracy measurement of the diffusion constant. All of these techniques require dedicated and costly instrumentation.

Standard fluorescence microscopy is widely used to observe lipid mono- and bilayers doped with fluorescent probes on a micrometer-length scale. Every observation is accompanied by photobleaching of the probe molecules because of the intense illumination. Usually this effect is regarded as a nuisance because it limits observation time, but it can be used to qualitatively determine the mobility of the system (see, for example, Nollert et al., 1995). The experimental procedure is to close the field stop and observe the same spot for some time. Photobleaching results in a continuous decrease in brightness. Diffusion of unbleached dye molecules into the illuminated area leads to a bright rim on the image. The rule of thumb is: the broader the bright rim, the higher the mobility of the tracer. This rule can be put on a solid basis and used to quantitatively determine diffusion constants of tracer molecules, as we will show in this paper.

Using a classical FRAP setup, the temporal decrease in the fluorescence intensity in a continuously illuminated area has been used to determine diffusion constants (Peters et al., 1981). This technique, called continuous fluorescence microphotolysis (CFM), never came into widespread use because the same setup as the one used for FRAP is needed, but extraction of the diffusion constant from the measured data is more complicated because two parameters, diffusion constant and rate of photobleaching, must be determined instead of one.

In contrast to CFM, which does integrate the intensity over the whole illuminated area, we analyzed the spatial concentration profile resulting from such a bleaching process and determined the rate of photobleaching separately.

Received for publication 15 August 1996 and in final form 18 December 1996.

Address reprint requests to Dr. Rudolf Merkel, Physics Department, Biophysics Group, Technische Universität München, D-85748 Garching, Germany. Tel.: 49-89-2891-2480; Fax: 49-89-2891-2469; E-mail: rmerkel@physik.tu-muenchen.de.

0006-3495/97/04/1701/10 $2.00

For the area of illumination, we chose an elongated rectangular slit. This choice of geometry allowed the theoretical treatment of the problem as a one-dimensional process. Moreover, it was well suited to the application of digital image-processing techniques. To our knowledge, this modification of the CFM technique has not been reported before. In the case of dye molecules drifting in a homogeneous electric field we already used this technique to determine the electrical charge of the fluorescent molecules in polymer-supported membranes (Dietrich and Tampé, 1995). For the drift-free case, an elaborate theoretical analysis of the process was necessary. Here we mathematically analyzed the spatial as well as the temporal evolution of the concentration of unbleached tracer molecules during a photobleaching experiment. For long bleaching times a simple analytical description of the profiles is given. It was used to measure the quotient of bleaching rate and diffusion coefficient. This ensured simple performance of the experiment because time-resolved measurements were not necessary. The technique will be of practical relevance because only a standard fluorescence microscope is needed and the optical imaging of the sample is not affected.

The technique is especially well suited to the study of planar mono- or bilayers, which are a widespread model system for the cellular plasma membrane and are studied in their own right (Sackmann, 1996; Tampé et al., 1996; Möhwald, 1990).

THEORY

In this type of experiment the quantity observed is the concentration of the fluorescent probe. Its evolution in time and space is described by the diffusion equation, with an additional term that describes photobleaching.

$$\frac{dc(x, y)}{dt} = D \cdot \nabla^2 c(x, y) - B(x, y) \cdot c(x, y), \qquad (1)$$

where c denotes concentration, D is the diffusion constant, ∇^2 is a two-dimensional Laplace operator, and $B(x, y)$ is the rate of photobleaching, which depends on the chemical nature of the dye, its environment, and most importantly on the light intensity. Photobleaching is assumed to be characterized by a single first-order rate constant. This holds for the probe used in our experiments, but must be checked for each experimental situation. The geometry is depicted in Fig. 1. The length of the illuminated stripe is large compared to its width. In the center region the diffusion process is one-dimensional. The rate of photobleaching is B_0 within the illuminated stripe, zero otherwise.

$$\frac{dc(x)}{dt} = D \cdot \frac{d^2c(x)}{dx^2} - B_0 \cdot \Theta(w - x) \cdot \Theta(x) \cdot c(x), \qquad (2)$$

where $\Theta(x)$ denotes the step function ($\Theta(x)$ is 1 for $x > 0$, zero otherwise), and w denotes the width of the illuminated stripe. Boundary conditions for Eqs. 1 and 2 are constant concentration c_0 at time 0 and vanishing flows at infinity.

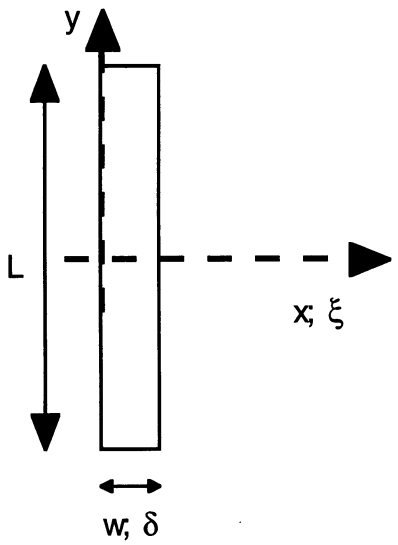

FIGURE 1 The coordinates used for the theory. The origin is at the left edge of the stripe at half-height. The y coordinate is along the length of the stripe, the x coordinate perpendicular. L and W denote the length and width of the stripe. Greek characters indicate dimensionless quantities: δ, width; ξ, x coordinate.

Furthermore, $c(x)$ and its first derivative with respect to x (proportional to the flux) must be continuous functions.

In the rest of this chapter we will first develop a rigorous solution for the infinitely broad stripe (the illuminated half-plane). Based on this, we will develop an approximate solution for finite width of the illuminated stripe. The validity of this approximation will be explored by direct numerical integration of Eq. 2.

Illuminated half-plane

First of all, dimensionless units are introduced. The natural time scale of Eq. 2 is the inverse of the bleaching rate B_0, and the natural length scale is $\sqrt{D/B_0}$. Concentrations are given in fractions of c_0. The dimensionless variables are

$$\begin{aligned} \tau &:= t \cdot B_0 \\ \xi &:= x/\sqrt{D/B_0}. \end{aligned} \qquad (3)$$

The diffusion equation for the illuminated half-plane in dimensionless units is

$$\frac{dc_\infty}{d\tau} = \frac{d^2c_\infty}{d\xi^2} - \Theta(\xi)c_\infty, \qquad (4)$$

Where $\Theta(x)$ is defined at Eq. 2 and c_∞ denotes the exact solution for the concentration of the infinitely broad illuminated stripe. Boundary conditions are $c_\infty(\xi, \tau = 0) = 1$ and vanishing flux at $\xi = \pm\infty$. The solution can be found by

Laplace transformation of Eq. 4 with respect to time (Luikov, 1968) (for details see Appendix 1). It is given by

$$c_\infty(\xi > 0, \tau) = e^{-\tau}\mathrm{erf}(\sqrt{\xi^2/(4\tau)}) + \int_0^1 \frac{e^{-\tau\sigma - \xi^2/(4\tau\sigma)}}{\pi\sqrt{\sigma(1-\sigma)}}\,d\sigma$$

$$c_\infty(\xi < 0, \tau) = \mathrm{erf}(\sqrt{\xi^2/(4\tau)}) + \int_0^1 \frac{e^{-\tau(1-\sigma) - \xi^2/(4\tau\sigma)}}{\pi\sqrt{\sigma(1-\sigma)}}\,d\sigma. \quad (5)$$

Here erf is the error function (Abramowitz and Stegun, 1970). The integral has no closed solution, but it can be handled numerically. For $\xi = 0$ the solution can be given in closed form:

$$c_\infty(\xi = 0, \tau) = e^{-\tau/2} \cdot I_0(\tau/2). \quad (6)$$

I_0 is the zeroth modified Bessel function of the first kind (Abramowitz and Stegun, 1970). Please note that right at the edge ($\xi = 0$) the concentration does not depend on the diffusion constant. In Fig. 2 the solutions $c_\infty(\xi, \tau)$ are plotted for various times. For longer times ($\tau > 4$) the solution inside the illuminated region can be approximated by

$$c_{\mathrm{app}}(\xi, \tau) = c_\infty(\xi = 0, \tau) \cdot e^{-\xi} + e^{-\tau}. \quad (7)$$

Only the form of the profile is stationary (monoexponential with a decay length of $\sqrt{D/B_0}$). The prefactor $c_\infty(\xi = 0, \tau)$ never approaches a stationary value, aside from the trivial limit of zero (see Eq. 6). This results from the well-known fact that the diffusion equation does not have stationary solutions in two or fewer dimensions (see, e.g., deGennes, 1982). Related phenomena are the divergence of the potential of an infinitely long charged wire (Purcell, 1965) and the failure of Stokes' equation to describe the viscous drag on an infinitely long cylinder (Lamb, 1932). All of these problems are described by the Laplace equation $\nabla^2 f = 0$, the solutions of which cannot be normalized in a space of two or fewer dimensions.

Approximate solution for finite width of the illuminated stripe

In the case of finite width of the illuminated stripe the method of Laplace transformation fails because the back-transform into the time domain proves to be intractable. Therefore we will use an approximate solution. To a first approximation this is given by using the solution of the illuminated half plane (Eq. 5) up to the middle of the illuminated stripe and then assuming mirror symmetry around the center of the stripe.

$$c(\xi, \tau) \approx c_\infty(\xi, \tau) \quad \text{for} \quad \xi < \delta/2$$

and

$$c(\xi, \tau) \approx c_\infty(\delta - \xi, \tau) \quad (8)$$

elsewhere.

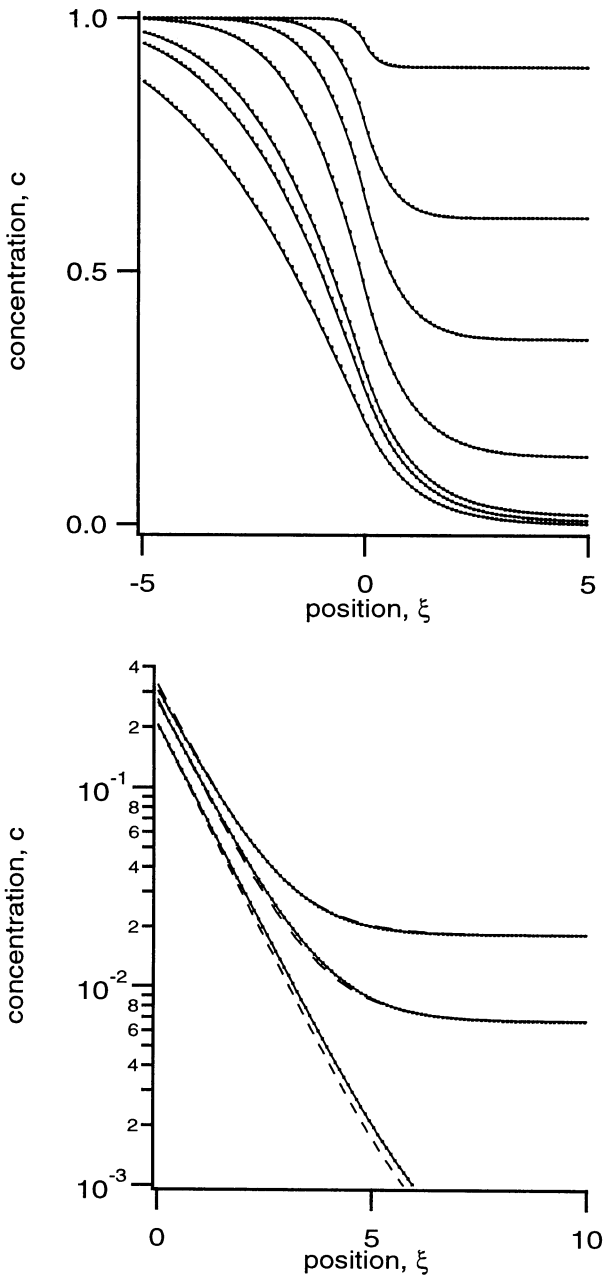

FIGURE 2 Concentration profiles for the illuminated half-plane. Solid lines represent analytical calculations (Eq. 5), dots the results of numerical integration of Eq. 2. (*Top*) Linear scale, dimensionless times: 0.1, 0.5, 1, 2, 4, 5, 8 (*from top to bottom*). (*Bottom*) Logarithmic scale, dimensionless times 4, 5, 8 (*from top to bottom*). Approximate profiles (Eq. 7; see text) are shown as dashed lines. Please note the different position scales.

Here δ is the width of the stripe in dimensionless units. This solution satisfies Eq. 2 for all boundary conditions. The only exemption is a discontinuity of the first derivative with respect to ξ at the center of the stripe. This corresponds to a flow j_{err} out of the illuminated stripe that is erroneous. For times less than roughly $\delta/2$, the influence is small. For longer times the influence of j_{err} can be approximately balanced by adding a further term to Eq. 8. (For a derivation

of this term see Appendix 2.)

$$c(\xi, \tau) \approx c_\infty(\xi, \tau) + e^{-\delta/2} \cdot c_\infty(\delta/2 - \xi, \tau) \quad \text{for} \quad \xi < \delta/2$$

and (9)

$$c(\xi, \tau) \approx c_\infty(\delta - \xi, \tau) + e^{-\delta/2} \cdot c_\infty(\xi - \delta/2, \tau)$$

elsewhere. To check the validity of these approximations we compared Eqs. 8 and 9 with direct numerical integration of the differential equation, Eq. 2. (For details of the numerical integration refer to Materials and Methods.) In Fig. 3 the case of a width of 5 is shown. For a dimensionless time of 1 Eq. 8 is a good approximation; for times of 3 and longer the additional term in Eq. 9 is necessary. At time 2 the solution is between the two approximations. For broader stripes the agreement is much better. For narrower stripes it gets worse. In the case of a stripe width of 3.2 and times larger than 3, Eq. 9 is still a good approximation, whereas Eq. 8 does not describe the data at any time (data not shown).

Within the range of times and widths used in the experiment, Eq. 9 describes the data very well. (Times ranged from 5.8 to 10, widths from 4 to 23. Both are given in dimensionless units.) With the use of Eq. 7 for c_∞, we find a concentration profile that is

$$c(\xi, \tau) \approx c_\infty(\xi = 0, \tau) \cdot \frac{\cosh(\xi - \delta/2)}{\cosh(\delta/2)} + e^{-\tau} \qquad (10)$$

within the illuminated stripe ($0 < \xi < \delta$)).

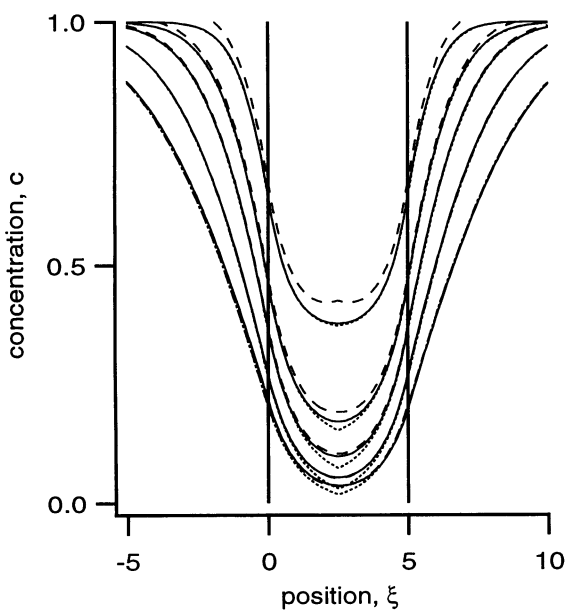

FIGURE 3 Concentration profiles for dimensionless times of 1, 2, 3, 5, and 8 (*from top to bottom*); the width of the illuminated stripe is 5. ——, Direct numerical integration of Eq. 2; ·····, Eq. 8; – – –, Eq. 9. The two vertical lines mark the borders of the illuminated stripe.

Immobile fraction

In FRAP studies it is often observed that a fraction of the probe molecules appear to be immobile (Axelrod et al., 1976). This can be modeled by the presence of two species of probe molecules. There is no conversion of mobile into immobile molecules or vice versa. The mobile fraction of concentration c_{mob} and diffusion constant D is described by the theory presented above. The immobile fraction of concentration c_{im} is characterized by a vanishing mobility. Thus the evolution of the immobile fraction is governed by the following equation:

$$\frac{dc_{im}(x, t)}{dt} = -B_{im} \cdot \Theta(x) \cdot \Theta(w - x) \cdot c_{im}(x, t), \qquad (11)$$

which is solved by

$$c_{im}(x, t) = c_{im,0} \quad \text{for} \quad 0 < x \quad \text{and} \quad x > w$$

and (12)

$$c_{im}(x, t) = c_{im,0} \cdot e^{-B_{im} \cdot t}$$

within the stripe.

$c_{mob}(x)$ must be a continuous function, because discontinuities would lead to infinite flows that are nonphysical. For $c_{im}(x)$ this boundary condition does not apply because there is no mobility. The complete solution is given by the sum of $c_{im}(x)$ and $c_{mob}(x)$ (the solution of Eq. 2).

Asymmetrical diffusion

In strongly damped systems, such as viscous fluids or lipid membranes, a force f applied to a particle will move it with constant velocity v. Both f and v are connected via the mobility M. Ordinary fluids are isotropic, and M is a scalar quantity. In more structured systems M will be a tensor of rank 2. In other words, f and v are no longer parallel. As long as the mobility tensor does not depend on force or velocity, Einstein's relation is valid and the passive motion of the particles is described by the diffusion equation. Equation 1 must be replaced by

$$\frac{dc(x_1, x_2, t)}{dt} = \sum_{i,j=1}^{2} D_{ij} \cdot \frac{\partial^2 c}{\partial x_i \partial x_j} - B(x_1, x_2) \cdot c, \qquad (13)$$

with $D_{ij} = k_B T M_{ij}$. For convenience we use the notation x_1 and x_2 instead of x and y. The bleaching geometry is unaltered.

$$B(x_1, x_2) = B_0 \cdot \Theta(x_1) \cdot \Theta(w - x_1). \qquad (14)$$

The resulting solution is constant in the x_2 direction and solves Eq. 2 in the x_1 direction, but with D replaced by D_{11}. Only the sum of the off-diagonal elements enters Eq. 13. This makes it possible to replace the off-diagonal elements by their mean value. In other words, the concentration profile depends only on the symmetrical part of the diffusion tensor. This matrix possesses two eigenvalues, D_1 and

D_2, with corresponding orthogonal eigenvectors. The measured diffusion coefficient D_{11} is related to the eigenvalues of the symmetrical part of the diffusion tensor via

$$D_{11} = p_1^2 \cdot D_1 + p_2^2 \cdot D_2, \quad (15)$$

where p_1 denotes the projection of the eigenvector belonging to D_1 onto the x_1 axis, and p_2 is defined analogously for D_2. Please note that the removal of the antisymmetrical part of D_{ij} is possible only as long as there are no external forces acting on the particles. In other words, to determine the full mobility tensor M_{ij}, application of external forces is necessary. With diffusion measurements only the symmetrical part can be measured.

MATERIALS AND METHODS

Experiments

Setup

A detailed description of the experimental setup has already appeared (Dietrich and Tampé, 1995). In summary, the lipid film preparations were placed in the image plane of an epifluorescence microscope (Kondensor V; Carl Zeiss, Jena, Germany). A high-pressure mercury arc lamp (HBO 50; Osram, Munich, Germany) served as the light source and was aligned for Köhler illumination. In the case of a continuous bleaching experiment, the round-field diaphragm was replaced by a slit. An objective with a long working distance (CD Plan 40, aperture 0.6; Olympus Optical, Hamburg, Germany) was used. For detection of the fluorescence the sensitive plate of a SIT camera (C 2400–08; Hamamatsu Photonics, Hamamatsu City, Japan) was placed in the image plane of the microscope. The pictures were recorded with standard video equipment. The video images were analyzed with a commercial image-processing system on a Macintosh computer (Macintosh Quadra 950, Apple Computer; equipped with Pixelstore and Pixelpipeline, Perceptics Corp., Knoxville, TN). The software used was Image VDM (Perceptics Corp.), based on the public domain software National Institutes of Health Image (Image 1.48; Wayne Rasband, National Institutes of Health). One pixel corresponded to an area of 0.405 μm $\times$ 0.405 μm on the specimen. Intensity values were digitized with 8-bit resolution. Control experiments with neutral density filters demonstrated a linear relationship between fluorescence intensity and gray levels of the image-processing system.

Lipid film preparation

The preparation of solid-supported lipid bilayers was performed as described previously (Merkel et al., 1989). A monolayer of L-α-dimyristoylphosphatidylcholine (DMPC) (Avanti Polar Lipids; Alabaster, AL) was transferred onto a plasma-cleaned glass slide by the Langmuir-Blodgett technique. The second lipid film was placed on the support by the Langmuir-Schäfer technique. This second layer was doped with 2 mol% *N*-(7-nitrobenz-2-oxa-1,3-diazol-4-yl)-dipalmitoylphosphatidylethanolamine (NBD-DPPE) (Molecular Probes, Eugene, OR). Depositions were performed at room temperature (~24°C) and at a lateral pressure of 20 mN/m.

Test for concentration quenching

One basic assumption in our approach is the proportionality of probe concentration and fluorescence intensity. Concentration quenching of the fluorescence probes could invalidate this assumption and lead to erroneous results (Robeson and Tilton, 1995). Concentration quenching shows up as deviation from linearity in a plot of intensity versus concentration. Lipid films with probe concentrations of 0.1, 0.5, 1.0, 2.0, 4.0, and 8.0 mol% were prepared as above. Fluorescence intensities were measured with a confocal laser scanning microscope (Odyssey XL; Noran Instruments, Middleton, WI). The excitation wavelength was 488 nm, and emission was detected at wavelengths of more than 515 nm. Intensities were averaged over an area of 400 μm^2. Great care was taken to use areas that were not scanned previously. The following gray-scale values were obtained: 10, 28, 56, 204, and 244 (in order of increasing probe concentrations). The relative error was estimated to be 10%. For probe concentrations of 4 mol% and less, the data fall on a straight line. At 8 mol% concentration, quenching plays a significant role. At probe concentrations of 2 mol% and less, the fluorescence images where homogeneous. At 4 mol% a slightly grainy structure was observed that was very pronounced at 8 mol%. Thus concentration quenching is accompanied by phase separation, but neither effect is present at the concentration used in our experiments (2 mol%).

Execution of experiments

In continuous bleaching experiments the ratio of the bleaching rate B_0 and the diffusion constant D was measured. To determine the diffusion constant, a separate measurement of the bleaching rate B_0 was necessary. The rate of photolysis was measured by analysis of the bleaching kinetics. This was done by illumination of the lipid layer within a circle of 180 μm diameter. The decay of fluorescence intensity was detected in its center as follows. At intervals the video signal was averaged for 0.33 s (eight video frames) to produce a time-averaged image. Sixteen hundred central pixels (square area of 16 $\times$ 16 μm = 40 $\times$ 40 pixels) of this image were used to perform a spatial averaging. The time course of the obtained mean values could be fitted with a single exponential function, as illustrated in Fig. 4 for two examples (*solid lines*). This demonstrated that photobleaching could be described with a first-order rate constant, the bleaching rate B_0. Simulations demonstrated that unbleached dyes diffusing into the center were of no relevance. Bleaching experiments with different intensities of excitation (and thus different rates of photobleaching) and repeated measurements of one sample showed that the error was less than 20%.

Determination of the quotient B_0/D was carried out by replacing the round diaphragm with a slit and performing a continuous bleaching experiment. When the fluorescence intensity in the illuminated stripe remained nearly constant, the slit was removed. The intensity profile was determined in an extension of about 160 μm perpendicular to the slit. (A typical fluorescence image is shown in Fig. 5.) To reduce noise, temporal and spatial averaging was carried out as follows. Twenty-four successive video frames (1 s) were averaged. An area of 400 $\times$ 60 pixels (162 $\times$ 23 μm, x $\times$

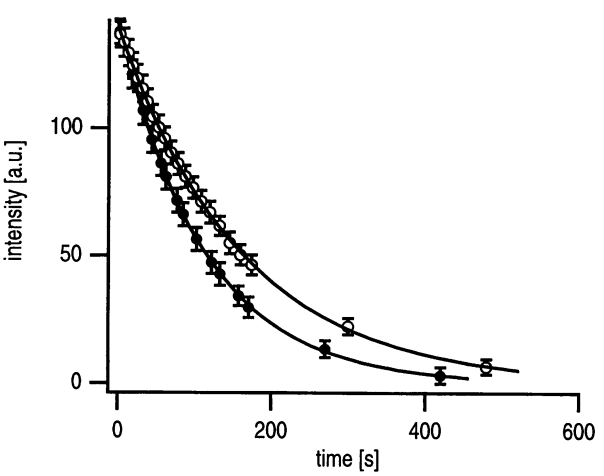

FIGURE 4 Decrease in the fluorescence intensity in the center of a continuously illuminated disc (diameter 180 μm) at 25°C (■) and 15°C (□). The exponents of the fitted exponential functions (——) equal the bleaching constant B_0. The results of all measurements of B_0 are summarized in Fig. 8.

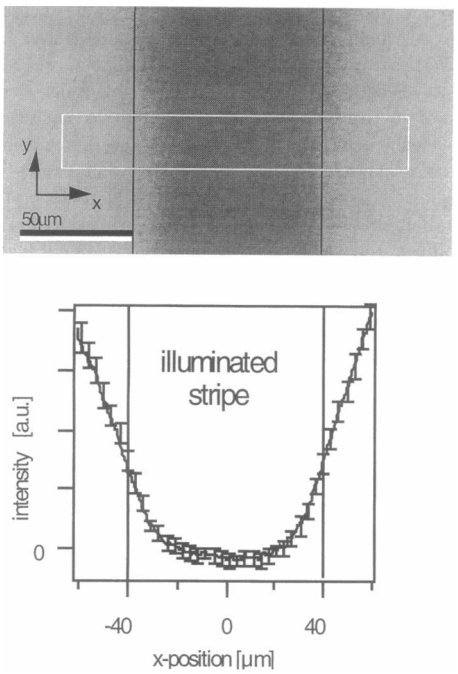

FIGURE 5 Determination of the bleaching profile (t_b = 12 min, τ = 7.2, δ = 5.6). The fluorescence micrograph (*top*) was obtained by averaging 24 successive video frames (1 s). The bright frame with dimension ($x \times y$) of 400 × 60 pixels (162 × 23 μm) indicates the area used for analysis of the profile. The pixels with the same x position were averaged and gave one point of the intensity profile (*bottom*). The error bars (shown for every fifth data point only) represent the standard deviation.

y) was used for analysis. Pixels with the same x position were averaged and gave one point of the intensity profile. The standard deviations of the data points were determined as well. An example of a recorded picture and the resulting concentration profile is given in Fig. 5. The time necessary to reach a sufficient approach to the analytical approximation (Eq. 10) depended on the experimental conditions. In practice, the bleaching time t_b was between 10 and 30 min, which corresponded to a characteristic time τ larger than 5. The slits used were about 90 μm wide.

Data analysis

Because of its simplicity, Eq. 10 formed the basis of our method of data evaluation. Substantial changes in image intensity during an experiment prohibited the determination of $c_\infty(\xi = 0, \tau)$, as the sensitivity of the camera had to be adjusted. Background fluorescence and stray light resulted in an additional constant. Thus the function used for fitting the experimental data in the continuously illuminated area was

$$c(x) = P_1 \cdot \cosh(\sqrt{B_0/D} \cdot (x - x_m)) + P_2, \qquad (16)$$

where P_1 and P_2 were general fit constants and x_m equaled the center of the stripe.

Measured intensity profiles were fitted with Eq. 16. χ^2 fitting following the procedure of Levenberg and Marquardt was used (Press et al., 1989). One fit parameter was the quotient of bleaching rate and diffusion coefficient (B_0/D). The experimentally determined standard deviations were used. To estimate the error, fits were performed with the relevant parameter B_0/D fixed, while all other parameters were allowed to vary. Variation of this parameter around the optimal value (minimum of the χ^2) resulted in an increase in the χ^2 value. A significant increase in χ^2 ($\Delta\chi^2 \approx 50\%$) was used to estimate the error of B_0/D.

Numerical calculations

Calculations

Numerical values of integrals that have no closed solution were calculated using Mathematica (Wolfram research, Champaign, IL) or self-developed programs, the accuracy of which was checked by comparison with Mathematica.

Simulations

For numerical calculations of concentration profiles, the Runge-Kutta algorithm of fourth order (Press et al., 1989) was used to integrate the reaction-diffusion equation (Eq. 2). (In this paper we discuss analytically or numerically calculated concentration profiles and fluorescence intensity profiles gained experimentally. To ensure clarity in language, we use the terms "simulation" and "calculation" in the first case, whereas "experiment" and "measurement" always relate to the second.) According to a bleaching experiment, the simulation started at constant dye concentration c_0. The size of the simulated system ensured that the central region was not affected by the borders. Comparison with analytically calculated concentration profiles for the illuminated half-plane revealed no significant deviations. Examples for calculated concentration profiles in the case of an illuminated stripe with finite width are given in Fig. 3 (*solid lines*). As in the case of measured profiles, calculated profiles were fitted with Eq. 16.

To determine how much time one has to wait until the analytical approximation (Eq. 16) yields correct results, simulations of continuous fluorescence photolysis experiments were performed. For the case of an illuminated stripe of finite width, calculations with different parameter sets of diffusion constant D and bleaching rate B_0 were performed. Fig. 6 shows the fitted values for B_0/D as a function of bleaching time for three examples. As predicted by the theory, profile analysis according to Eq. 16 provided reasonable results for bleaching times $\tau > 4$. The significance of the fits was investigated by adding random numbers (noise) to the calculated profiles and analyzing the distribution of the gained results (data not shown). For practical realization of the experiments, it was important to note that for long bleaching times the quality of the measurements decreased. Although the gained results of data analysis for noise-free profiles

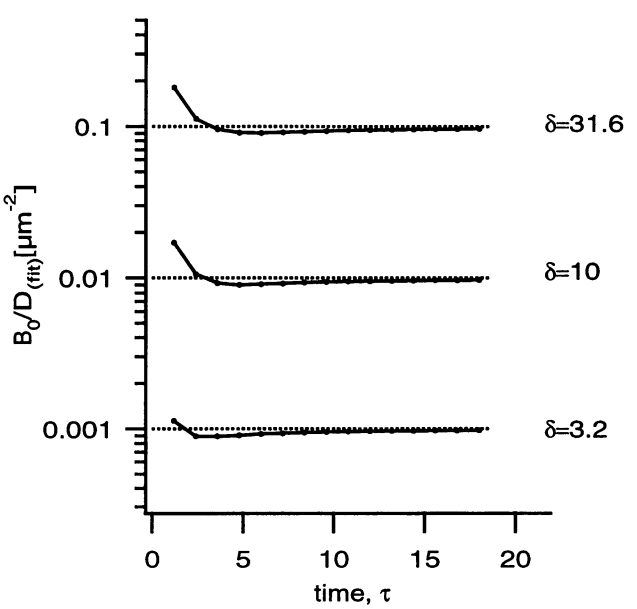

FIGURE 6 Profiles were numerically generated and then fitted with Eq. 16. The resulting parameter B_o/D is shown as a function of bleaching time τ. The dimensionless stripe width δ is indicated at each curve. Dashed lines indicate the values of the quotient B_o/D used for generation.

approached the "true" value for prolonged times, the errors associated with the analysis increased with time, reflecting the deterioration of the signal-to-noise ratio.

Diffusion measurements

As prototype experiments the temperature dependence of the diffusion of NBD-DPPE was measured in a supported DMPC bilayer on glass. Because of the main phase transition of the lipid, a substantial change in the diffusion constant was reported in the temperature range between 25°C and 15°C (Merkel et al., 1989). The measurements described here were made in the following order: 24.6°C, 25.2°C, 23.3°C, 22.2°C, 20.1°C, 18.4°C, 14.9°C, and 25°C. For direct comparison, standard FRAP measurements were performed between the first two measurements at 25.3°C. During the experiments the temperature was controlled and adjusted by a Peltier thermostat with an accuracy of ±0.5°C. At every temperature the bleaching constant B_0 and the quotient B_0/D were determined in separate experiments (cf. Materials and Methods). Three typical intensity profiles recorded in continuous bleaching experiments are shown in Fig. 7, and two examples of the bleaching kinetics are given in Fig. 4. Fig. 8 summarizes all experimental results. Both the bleaching constant B_0 and the diffusion constant D (Fig. 8, *top* and *bottom*, respectively) showed a strong temperature dependence. The bleaching rate decreased by nearly 50% and the diffusion constant dropped drastically (by nearly 2 orders of magnitude) in this temperature range. The results of the continuous bleaching method for the diffusion constant were in very good agreement with FRAP measurements and results reported previously (Merkel et al., 1989; Tamm and McConnell, 1985; Kühner et al., 1994). The temperature dependence of the bleaching rate can be understood as follows. Photobleaching occurs because of oxidation of the excited dye molecule (Slavik, 1994). The collision rate of molecular oxygen with the excited dye molecules determines the rate of bleaching. This collision rate has been investigated experimentally using electron spin resonance (ESR) in DMPC vesicles with a spin label in the headgroup region (TEMPO choline phosphatidic acid ester) (Subczynski et al., 1989). With decreasing temperature, a reduction in the collision rate by a factor of 2 for every 20° centigrade was found. This is comparable to our finding for the bleaching rate. However, a sudden decrease by a factor of 2 was found due to the main phase transition. This is absent in our data. The explanation might be one or a combination of the following facts: supported bilayers show more defects than vesicles (Sackmann, 1996; Tampé et al., 1996), their thermal expansion is at least partially suppressed, and the fluorescent probe used in our study is bulkier than the spin label.

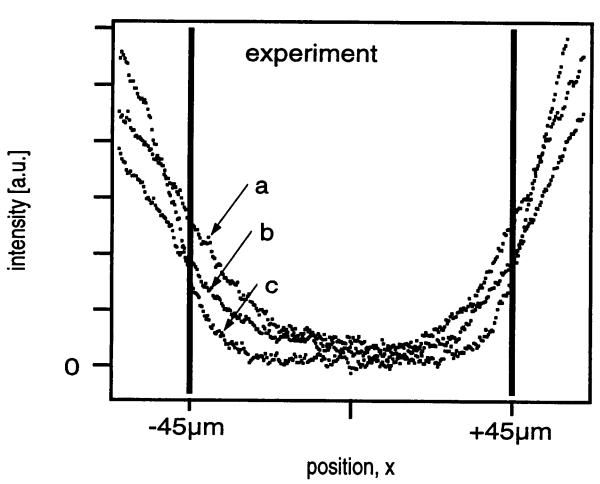

FIGURE 7 Examples for measured bleaching profiles of NBD-DPPE in a supported DMPC bilayer at different temperatures. *a*, 25.3°C: t_b = 11 min; τ = 9.2, δ = 4.9; *b*, 22°C: t_b = 17 min; τ = 8, δ = 5.6; *c*, 18°C: t_b = 25 min; τ = 10, δ = 13.7). The results of all measurements are displayed in Fig. 8.

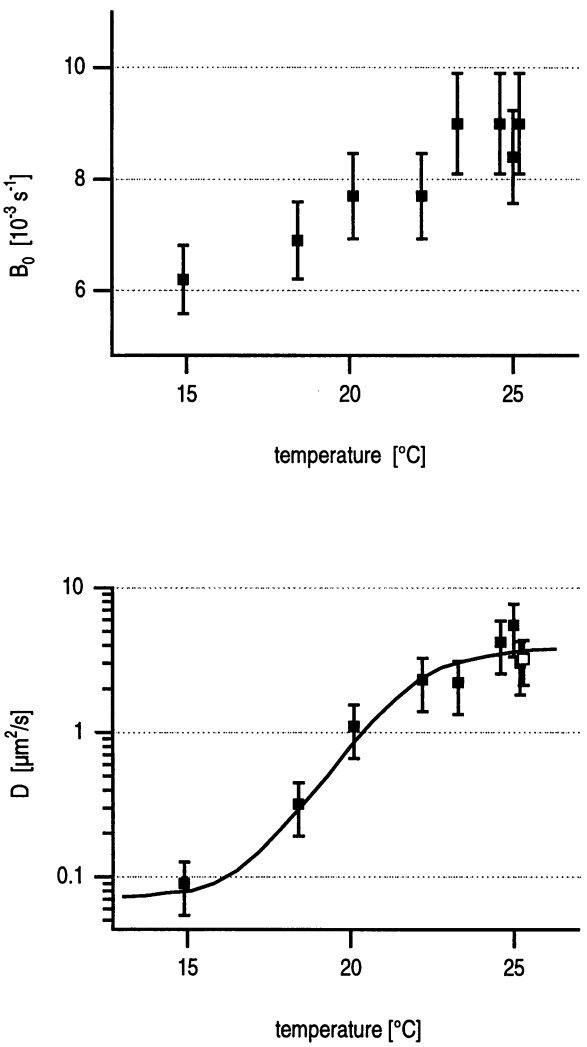

FIGURE 8 Temperature dependence of the rate of photolysis B_0 (*top*) and diffusion constant D (*bottom*) of DPPE-NBD in a supported DMPC bilayer (see Materials and Methods). Between the first two measurements, eight FRAP measurements were carried out at 25.2 ± 0.5°C. The open marker indicates the average value of these measurements and the error bar represents the standard deviation. The solid line is intended as a guide for the eye.

DISCUSSION AND CONCLUSION

Throughout this work we determined the bleaching constant and the ratio B_0/D in separate measurements with different geometries. This was dictated by the need to establish that the bleaching kinetics is monoexponential. Deviations from single exponential bleaching are expected in cases in which the probe molecules are located in nonequivalent microenvironments, as for example in randomly labeled proteins. Once this is established, the experiments could be performed in a simpler way: recording of the profiles of the illuminated slit from the beginning would be enough. In the initial phase of bleaching the innermost parts of the stripe

are not influenced by diffusion. The initial rate of intensity loss in the center of the stripe directly yields the bleaching rate. The quotient B_0/D would be subsequently determined as described above by the slope of the intensity variation from the boundary into the illuminated slit.

Other possible pitfalls are concentration quenching of the probe molecule and phase separation. Concentration quenching would result in a nonlinear dependence of fluorescence intensity on probe concentration and should lead to deviations from a monoexponential bleaching kinetics. We showed that neither effect plays a role in our experiments, but this must be checked for every system under study. Another possible complication is biphasic diffusion. Spatial variations of diffusion constant or bleaching rate are easily detected if they occur on a micron-length scale. If the length scale of this inhomogeneity cannot be resolved by light microscopy, only an average diffusion coefficient can be determined. There is no way to detect the presence of submicroscopic inhomogeneity. This holds as well for FRAP. In cases in which inhomogeneities are visible, a determination of the diffusion constant is not possible with our approach. The presence of two species with different mobilities is also extremely difficult to evaluate. Theoretically, if both species are bleached with equal rates, a fit using two cosh functions with different length scales would yield both diffusion constants. In practice, the quality of the data will make futile any such attempt at a fit. Moreover, different bleaching rates are expected. In that case, extraction of the diffusion constants will be impossible. The presence of an immobile fraction can be easily handled. We evaluate the intensity profile within the illuminated slit only. There the concentration of the immobile fraction is spatially constant (Eq. 12) and will be absorbed by the fitting constant P_2 in Eq. 16. Thus the resulting diffusion constants are not influenced by an immobile fraction. The presence of an immobile fraction would lead to a discontinuity of the concentration (and thus the fluorescence intensity) at the borders of the illuminated slit (Eq. 12). As we measure after several bleaching times, the concentration of immobile probes within the slit will be extremely low. Therefore the immobile fraction is simply the magnitude of the discontinuity of the fluorescence intensity at the borders of the illuminated stripe normalized by the fluorescence intensity at the beginning of the experiment. (The immobile fraction is defined as $c_{0,\mathrm{im}}/(c_{0,\mathrm{im}} + c_{0,\mathrm{mob}})$.) No serious attempt to measure the immobile fraction was made.

One major advantage of this technique is its low demand on equipment. A standard fluorescence microscope, a sensitive camera, a video recorder, and a computer with a digital image processing board are needed. All of these items are likely to be found in a biosciences laboratory and can serve multiple purposes. There is no need for costly and delicate ion lasers and photon counters. Moreover, no dedicated optical setup is needed. Virtually no time-consuming alignment of optics is necessary.

There are several additional advantages. First of all, drift can easily be detected by an asymmetrical intensity profile. Moreover, spatial variations in the diffusion constant or bleaching rate are readily detected. Asymmetrical diffusion can be detected by rotating either the illuminated stripe or the sample. Fitting the measured diffusion constants as a function of rotation angle by Eq. 15 allows determination of the eigenvalues of the symmetrical part of the diffusion tensor and the corresponding directions on the sample, which are the eigenvectors. Another obvious advantage of the method is that the needed time resolution is moderate, and averaging can be used to improve the signal-to-noise ratio. Analogous to a FRAP experiment, the size of the illuminated area can be adapted to optimize the performance of the experiment. The bleaching rate is a further parameter that allows tuning of the measurement in principle. However, because we used a simple HBO 50, it was not advisable to use any additional neutral density filters, which would have led to an increase in the necessary bleaching time. A possible way to increase the rate of photolysis would be enrichment of the sample with molecular oxygen. This would make photooxidation more likely.

The range of diffusion constants that can be measured is limited to high values by the highest width of the illuminated stripe that can be homogeneously illuminated and by the bleaching constant B_0. Inserting typical values ($w = 100$ μm, $B_0 = 0.008$ 1/s) and demanding that the dimensionless width (see Eq. 3) must be at least 3.2 leads to an upper limit of 8 $\mu m^2/s$. The bound for low values is given by the spatial resolution. The dimensionless decay length must be represented by several pixels, which leads to a lower bound of 0.04 $\mu m^2/s$. We must stress that both boundaries depend, in a very sensitive way, on the setup. The bound for low values could be improved by at least a factor of 10 by using a higher magnification on the camera or introducing neutral density filters. The upper bound can be improved by using a different optical setup. Using identical samples but a different microscope (Axiovert 135TV, equipped with a high-pressure mercury arc lamp HBO 100 as the light source and an objective Fluar 40×/1.30 oil; Carl Zeiss, Jena, Germany), we found a bleaching rate B_0 of 0.17 1/s. This is higher by a factor of 20 than the value obtained with the setup used in the rest of our experiments. Therefore diffusion constants up to 100 $\mu m^2/s$ could be measured with this different setup. With this apparatus we were able to use a standard CCD camera (C5403; Hamamatsu), even at probe concentrations of 1 mol%. Thus given a state-of-the-art microscope, even a highly sensitive camera might be unnecessary.

There are several reasons for the error of 40% that is estimated for the diffusion measurements of supported DMPC bilayers. First, two separate experiments are necessary to determine D (B_0 and B_0/D), leading to a summation of the errors. Second, the error in the determined value B_0/D must be estimated carefully (50% increase in the optimal χ^2 value). The statistics of the normalized residues of the optimal fits reveal a correlation between neighbored data points (correlation length in the range of 10 μm; data not shown). This is not surprising because a disturbance (for

example, a defect in the lipid layer preparation) affects the spatial surrounding, and therefore measurements of the fluorescence intensity of neighbored points cannot be expected to be statistically independent. Moreover, the experimental profiles in Fig. 7 show a slight asymmetry, which is probably due to less than ideal illumination, which leads to a systematic error. Please note that data analysis is only necessary in the illuminated part of the profiles.

Furthermore, the experimental procedure of destroying fluorescent molecules (signal) leads to only limited signal-to-noise ratios. As already addressed in the results, there is an optimal time when the approach to a profile following Eq. 16 is sufficient and the signal-to-noise ratio is still good. As estimated, this holds for bleaching times τ of about 5 to 10, which corresponded to times between 10 and 30 min for our samples.

With optimal adaptation of the different experimental parameters, the technique could be improved with regard to accuracy and duration. The rate of photolysis can be controlled by variation of illumination intensity (neutral density filters), and the width of the illuminated stripe by an adapted diaphragm or optics. Data analysis that additionally takes into account the temporal development of the induced profiles allows the determination of the experimental parameter with higher accuracy and would avoid a separate determination of the bleaching constant B_0. However, this creates the need for a specialized setup. We have used the technique in the less optimized form. Although the data are less accurate (but compare the error bars for FRAP and our technique in Fig. 8), the results are often very helpful, because they are gained in addition to standard optical imaging (Behrisch et al., 1995) without much higher experimental effort. We believe that the main virtues of the method are its simplicity and relatively low demands on specialized equipment.

APPENDIX 1

The solution of Eq. 4 by Laplace transformation is obtained as follows. The operation of Laplace transformation is defined by (Doetsch, 1947)

$$L[f(t)] := \int_0^\infty e^{-st} f(t)\mathrm{d}s = f(s). \tag{A1}$$

Using the relation

$$L\left[\frac{\mathrm{d}f}{\mathrm{d}t}\right] = s \cdot f(s) - f(t=0), \tag{A2}$$

we derive the following equation for the transformed concentration $c_\infty(\xi, s)$:

$$s \cdot c_\infty - 1 = D\frac{\mathrm{d}^2 c_\infty}{\mathrm{d}\xi^2} - \Theta(\xi) \cdot c_\infty. \tag{A3}$$

It is straightforward to construct solutions for Eq. A3 in both half-planes. The integration constants are determined so that the boundary conditions at $\pm\infty$ are fulfilled and concentration and flux are continuous at $\xi = 0$. The solution is given by

$$\begin{aligned} c_\infty(\xi > 0, s) &= \frac{1}{s+1} + \left(\frac{1}{\sqrt{s(s+1)}} - \frac{1}{s+1}\right) e^{-\sqrt{s+1}\xi} \\ c_\infty(\xi < 0, s) &= \frac{1}{s} + \left(\frac{1}{\sqrt{s(s+1)}} - \frac{1}{s}\right) e^{-\sqrt{s}\xi}. \end{aligned} \tag{A4}$$

What remains to be done is the back-transform into the time domain. It cannot be given in closed form. Using the convolution theorem (Doetsch, 1947) and tabulated transforms, Eq. 5 is reached.

APPENDIX 2

Here we present a justification for the correcting term (Eq. 9) to the concentration profiles. The magnitude of the erroneous flow j_{err} can be analyzed by differentiating Eq. 5. We find that the ratio of j_{err} to j_0, the flux into the stripe at its border ($\xi = 0$ or $\xi = \delta$), starts at zero and reaches a plateau, the amplitude of which is given by $e^{-\delta/2}$. It is reached roughly within $\delta/2$ time units. This is expected from the above approximation (Eq. 7). It shows that at a distance α from the edge of the illuminated stripe, for approximately the first α time units, the dye molecules are bleached exponentially before the flux of particles from the dark half-plane takes over and the profile crosses over to $e^{-\alpha} \cdot c_\infty(\xi = 0, \tau)$. $\mathrm{d}c_\infty/\mathrm{d}\xi|_{\xi=0}$ approaches $c_\infty(\xi = 0, \tau)$ within a few dimensionless time units (for example, at $\tau = 4$ the error is only 9%; it drops as $1/\tau$). Thus we expect the plateau value of $e^{-\delta/2}$ for the ratio of j_{err} and j_0. For dimensionless times less than $\delta/2$, Eq. 8 is a good approximation for the true concentration profile. For longer times the erroneous flux j_{err} must be balanced by a source of particles at the center of the stripe with strength $-j_{\mathrm{err}}$. We shall see that this additional term is a small correction for widths of the illuminated stripe in the experimental range (δ ranges from 4 to 23). Therefore we can make the additional approximation that the ratio of j_{err} and j_0 is constant and equals $e^{-\delta/2}$ for all times. A concentration profile that corresponds to that influx into an illuminated region is given by $e^{-\delta/2} \cdot c_\infty(\xi)$. This is exactly the additional term in Eq. 9. The shift of the coordinates in Eq. 9 is necessary to place this source of particles at the center of the illuminated stripe.

We thank Dr. Martin Kühner for carrying out the FRAP measurements and Marius Dichtl and Melanie Hohnadel for help with the confocal microscope. We are greatly indebted to Erich Sackmann for the chance to perform this study in his laboratories and for helpful discussions.

This work was supported by the Bundesminister für Bildung und Forschung (BMBF 0310851) and the Deutsche Forschungsgemeinschaft (Sonderforschungsbereich 266). One of the authors (CD) is grateful for the support of a European Union scholarship.

REFERENCES

Abramowitz, M., and I. A. Stegun. 1970. Handbook of Mathematical Functions. Dover Publications, New York, London.

Axelrod, D., D. E. Koppel, J. Schlessinger, E. L. Elson, and W. W. Webb. 1976. Mobility measurements by analysis of fluorescence recovery kinetics. *Biophys. J.* 16:1055–1096.

Behrisch, A., C. Dietrich, A. A. Noegler, M. Schleicher, and E. Sackmann. 1995. The actin-binding protein Hisactophilin binds in vitro to partially charged membranes and mediates actin coupling to membranes. *Biochemistry.* 34:15182–15190.

Cherry, J. R. 1979. Rotational and lateral diffusion of membrane proteins. *Biochim. Biophys. Acta.* 559:289–327.

deGennes, P. G. 1982. Kinetics of diffusion-controlled processes in dense polymer systems. I. Nonentangled regimes. *J. Chem. Phys.* 76: 3316–3326.

Dietrich, C., and R. Tampé. 1995. Charge determination of membrane molecules in polymer-supported lipid layers. *Biochim. Biophys. Acta.* 1238:183–191.

Doetsch, W. 1947. Tabellen zur Laplace Transformation und Anleitung zum Gebrauch. Springer Verlag, Berlin.

Jacobson, K., D. S. Sheets, and R. Simson. 1995. Revisiting the fluid mosaic model of membranes. *Science.* 268:1441–1442.

Kühner, M., R. Tampé, and E. Sackmann. 1994. Lipid mono- and bilayer supported on polymer films: composite polymer-lipid films on solid substrates. *Biophys. J.* 67:217–226.

Lamb, H. 1932. Hydrodynamics. Cambridge University Press, Cambridge.

Luikov, A. V. 1968. Analytical Heat Diffusion Theory. Academic Press, New York, London.

Merkel, R., E. Sackmann, and E. Evans. 1989. Molecular friction and epitactic coupling between monolyers in supported bilayers. *J. Phys. France.* 50:1535–1555.

Miehlich, R., and H. Gaub. 1993. Holographic pattern photobleaching apparatus for measurement of lateral transport processes at interfaces—design and performance. *Rev. Sci. Instrum.* 64:2632–2638.

Möhwald, H. 1990. Phospholipid and phosphopholipid-protein monolayers at the air/water interface. *Annu. Rev. Phys. Chem.* 41:441–476.

Nollert, P., H. Kiefer, and F. Jähnig. 1995. Lipid vesicle adsorption versus formation of planar bilayers on solid surfaces. *Biophys. J.* 69: 1447–1455.

Peters, R., and K. Beck. 1983. Translational diffusion in phospholipid monolayers measured by fluorescence microphotolysis. *Proc. Natl. Acad. Sci. USA.* 80:7183–7187.

Peters, R., A. Brünger, and K. Schulten. 1981. Continuous fluorescence microphotolysis: a sensitive method for study process in single cells. *Proc. Natl. Acad. Sci. USA.* 78:962–966.

Press, W. H., B. P. Flannery, S. A. Teukolsky, and W. T. Vetterling. 1989. Numerical Recipes in C, 2nd Ed. Cambridge University Press, Cambridge.

Purcell, E. M. 1965. Electricity and Magnetism. Berkeley Physics Course, Vol. 2. McGraw-Hill Book Company, New York.

Robeson, J. L., and R. D. Tilton. 1995. Effect of concentration quenching on fluorescence recovery after photobleaching measurements. *Biophys. J.* 68:2145–2155.

Sackmann, E. 1996. Supported membranes: scientific and practical applications. *Science.* 271:43–48.

Slavik, J. 1994. Fluorescent Probes in Cellular and Molecular Biology. CRC Press, Boca Raton, FL.

Smith, B. A., and H. M. McConnell. 1978. Determination of molecular motion in membranes using periodic pattern photobleaching. *Proc. Natl. Acad. Sci. USA.* 75:2759–2763.

Subczynski, W. K., J. S. Hyde, and A. Kusumi. 1989. Oxygen permeability of phosphatidyl-cholesterol membranes. *Proc. Natl. Acad. Sci. USA.* 86:4474–4478.

Tamm, L. K., and H. M. McConnell. 1985. Supported phospholipid bilayers. *Biophys. J.* 49:105–113.

Tampé, R., C. Dietrich, S. Gritsch, G. Elender, and L. Schmitt. 1996. Biofunctionalized membranes on solid surfaces. *In* Nanofabrication and Biosystems: Frontiers and Challenges. H. C. Hoch, L. W. Jelinski, and H. G. Craighead. Cambridge University Press, Cambridge. 201–221.

Thompson, N. L., T. P. Burghardt, and D. Axelrod. 1981. Measuring surface dynamics of biomolecules by total internal reflection fluorescence with photobleaching recovery of correlation spectroscopy. *Biophys. J.* 33:435–454.

Vaz, W. L. C., R. M. Clegg, and D. Hallmann. 1985. Translational diffusion in liquid crystalline phase phosphatidylcholine multibilayers. A comparison of experiment with theory. *Biochemistry.* 24:781–786.

Wedekind, P., U. Kubitschek, and R. Peters. 1994. Scanning microphotolysis: a new photobleaching technique based on fast intensity modulation of a scanned laser beam and confocal imaging. *J. Microsc.* 176:22–33.